

Facile Decoration of Polyaniline Fiber with Ag Nanoparticles for Recyclable SERS Substrate

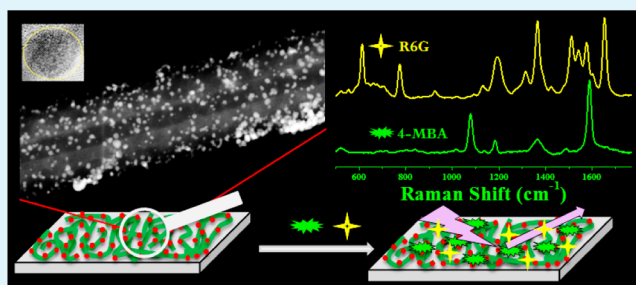
Sanjoy Mondal, Utpal Rana, and Sudip Malik*

Polymer Science Unit, Indian Association for the Cultivation of Science, 2A and 2B Raja S. C. Mullick Road, Jadavpur, Kolkata 700032, India

S Supporting Information

ABSTRACT: Facile synthesis of polyaniline@Ag composite has been successfully demonstrated by a simple solution-dipping method using high-aspect-ratio benzene tetracarboxylic acid-doped polyaniline (BDP) fiber as a nontoxic reducing agent as well as template cum stabilizer. In BDP@Ag composite, BDP fibers are decorated with spherical Ag nanoparticles (Ag NPs), and the population of Ag NPs on BDP fibers is controlled by changing the molar concentration of AgNO₃. Importantly, Ag-NP-decorated BDP fibers (BDP@Ag composites) have been evolved as a sensitive materials for the detection of trace amounts of 4-mercaptobenzoic acid and rhodamine 6G as an analyte of surface-enhanced Raman scattering (SERS), and the detection limit is down to nanomolar concentrations with excellent recyclability. Furthermore, synthesized BDP@Ag composites are applied simultaneously as an active SERS substrate and a superior catalyst for reduction of 4-nitrothiophenol.

KEYWORDS: polyaniline, Ag nanoparticles, SERS, recycle, 4-NTP reduction



INTRODUCTION

Surface-enhanced Raman scattering (SERS) is a powerful and attractive spectroscopic technique for the detection of ultra-sensitive and very low concentration analyte (chemical and biological) molecules at the metal surface because it demonstrates the single-molecule fingerprint-vibration information.^{1–3} Primarily, SERS is observed for analytes adsorbed onto a coinage-metal surface (Au, Ag, etc.) with the excitation near the visible region. Noble-metal nanoparticles (such as Au, Ag, Pt, and Pd) have attracted importance recently because of their promising many-field applications like sensing,^{4,5} medical,^{6,7} optical,^{8,9} and electronic devices^{10,11} as well as catalyst^{12,13} because their properties greatly depend on their size, surface structure, and composition.^{8,9,14} Au and Ag nanoparticles have unique features of localized surface plasmon resonance,^{15–17} resulting in excellent activity and good sensitivity as a SERS substrate. SERS is extremely dependent on the interaction between adsorbed molecules (analyte) and the surface of plasmonic nanostructures (substrate such as Au and Ag nanostructures).^{17,18} Making of active SERS substrate is an important job; presently, there are several types of substrate design being investigated such as porous substrates,¹⁹ metal nanoparticle films,²⁰ and metallic and bimetallic nanostructures.^{21,22} Planar metal substrate has lower activity rather than small nanostructure toward SERS sensitivity/activity because of its limitation as a “hot spot” in a substrate.²³ Cost-effective and easily reusable substrate preparation is also an important and challenging task for SERS applications.^{14,24–29}

Although UV–vis absorption spectroscopy for monitoring the catalytic reduction of 4-nitrophenol (4-NP) is well-developed,^{30–35} it does not provide all chemical information about the molecule during a reaction. So compared to this technique, SERS is an excellent technique for monitoring such catalytic reaction because it is surface-selective and can generate single-molecule information.^{30–32} The design of a bifunctional system combining both catalytic and SERS activity provides new insights into the mechanism, kinetic and structural evolution of catalytic reactions by Raman spectroscopy. To apply this technique in monitoring the catalytic activity, the synthesized composite should act both like a catalyst and also like a SERS substrate material. There are several reports on catalytic reaction catalyzed by nanoparticles that are SERS inactive.^{12,13,36} Therefore, to overcome this problem, noble-metal nanoparticles are fabricated on polymer/semiconductor matrix in such a way that nanocomposites act as a catalyst as well as an active SERS substrate.

Nowadays, polymer–noble-metal or semiconductor–noble-metal nanocomposites have received a great deal of attention owing to their excellent physical and chemical properties as well as the possibility of applications in the fields of catalysis, electronic devices, etc.^{8–13} Among the conducting polymers, polyaniline (PANI) is very important for metal-incorporated nanostructure formation, owing to the presence of many –NH

Received: February 27, 2015

Accepted: April 26, 2015

Published: April 27, 2015

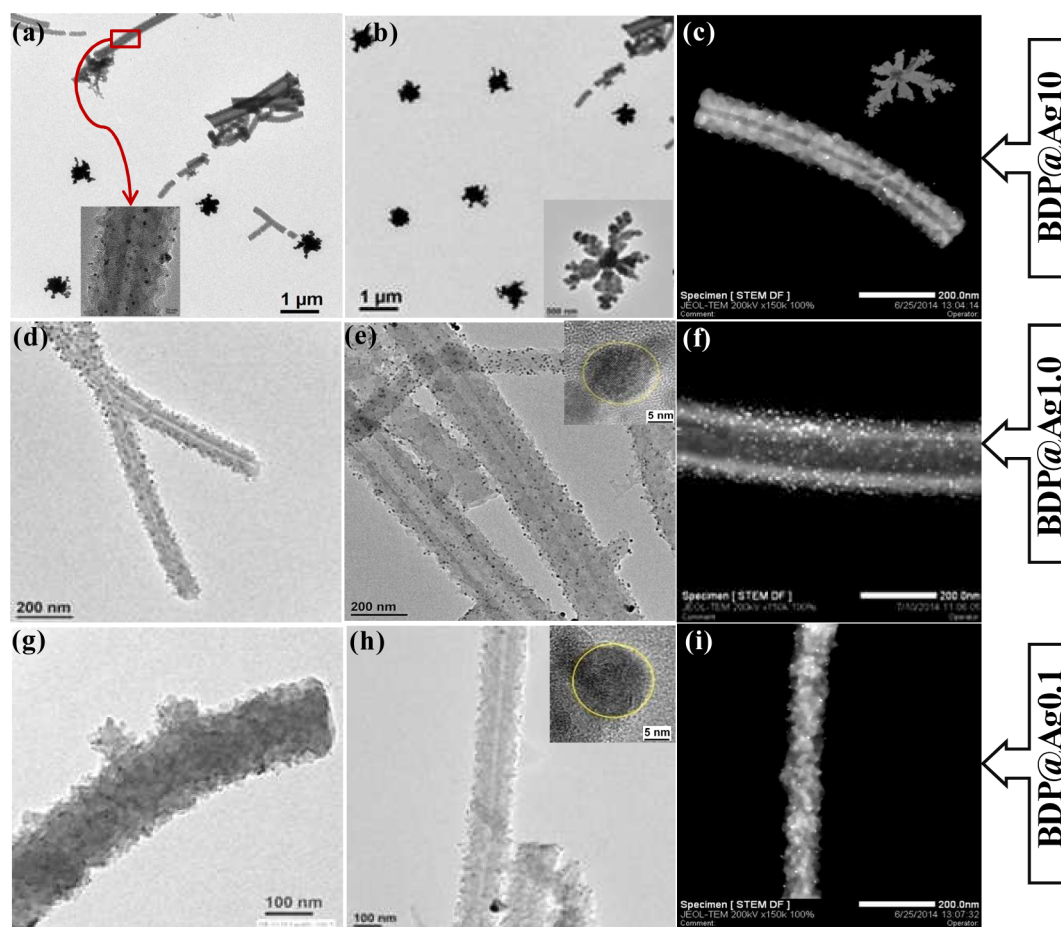


Figure 1. Effect of Ag nanoparticle loading on the BDP matrix: BDP@Ag10 composite, (a) TEM image, (b) bright-field image, and (c) dark-field image; BDP@Ag1.0 composite, (d and e) bright-field images and (f) dark-field image; BDP@Ag0.1 composite, (g and h) bright-field image and (i) dark-field image.

groups in the polymer chain.^{37–41} Another advantage of PANI lies with its reduction potential, which is relatively higher than that of the common noble metal, that results the facile formation of metal nanoparticles at room temperature. PANI itself plays a dual role during nanoparticle formation as a binding agent and also as reducing agent. Apart from these, PANI also offers good thermal and environmental stability, coupled with excellent electrical, electrochemical, and optical properties.^{40,41}

In this article, we have reported a simple straightforward synthesis of Ag nanoparticles (Ag NPs) decorated on PANI fibers by a solution-dipping technique. Synthesized composites have been characterized by HRTEM, XPS, XRD, UV–vis, FTIR, and TGA studies. Morphological changes and the population of Ag NPs on BDP fiber have been checked. Synthesized BDP@Ag composites have been used as an active/sensitive SERS substrate for detection of small molecules like 4-mercaptobenzoic acid (4-MBA), rhodamine 6G (R6G), and 4-nitrothiophenol (4-NTP) when they are present below nanomolar concentration level. Furthermore, BDP@Ag composites have been tested for dual activity as a catalyst as well as an active SERS substrate utilizing 4-NTP.

EXPERIMENTAL SECTION

Materials. Aniline (Merck Chemicals) was distilled under reduced pressure and stored at 5 °C in a dark place. Silver nitrate (AgNO_3), 1,2,4,5-benzenetetracarboxylic acid (BTCA), and ammonium persulfate

[(NH_4)₂S₂O₈] (APS) were purchased from Sigma-Aldrich and were used without further purification. 4-MBA, R6G, and 4-NTP were purchased from TCI Chemicals (India) Pvt. Ltd.

Instruments. Bright-field and high-angle annular dark-field (HAADF) imaging and mapping of BDP@Ag composites were carried out on a UHR-FEG-TEM (JEOL, JEM 2100F) instrument at an accelerating voltage of 200 kV. Samples were spread over a 200 mesh Cu-grid coated with a holey-carbon support film. UV–vis spectra of composites were recorded by using a UV–vis spectrophotometer from Agilent (model 8453) in a quartz cell with path length of 1.0 cm. FTIR spectroscopy of BDP@Ag composites was carried out on a FTIR-8400S instrument (Shimadzu) using KBr pellets. Powered XRD analysis was performed by using a Bruker AXS diffractometer (D8 advance) using $\text{Cu K}\alpha$ radiation ($\lambda = 1.542 \text{ \AA}$), a generator voltage of 40 kV, and a current of 40 mA. Samples were scanned typically from 10 to 85° at the rate of 0.5 s/step with a step width of 0.02. XPS analysis of BDP@Ag composite was performed by using a focused monochromatized Al $\text{K}\alpha$ X-ray source (1486.8 eV) in an Omicron Nano Technology 0571 XPS instrument. Thermogravimetric analyses (TGA) were done by a TA thermal analysis system. Samples were scanned from 25 to 800 °C with a heating rate of 10 °C/min under N_2 atmosphere. The amount of Ag present in the BDP@Ag composites was measured by an Optima 2100 DV (PerkinElmer) inductively coupled plasma atomic-emission spectroscopy (ICP-AES) instrument. SERS measurements were performed with a Raman triple spectrometer (model T-64000, Horiba-Jobin Yvon) fitted with a synapse detector. The samples were excited with a 514.5 nm laser (Spectra Physics, model Stabilite 2017). I – V relationship of synthesized composite was measured by using Keithley 0617 electrometer with two-probe methods at room temperature. EPR

spectra were recorded with a JEOL JES-FA200 spectrometer at room temperature.

Synthesis of High-Aspect-Ratio PANI Fiber. The synthesis of high-aspect-ratio PANI fiber was reported in our earlier report.³⁹ In a typical reaction, BTCA (0.07 g, 0.27 mmol) was dissolved in 15 mL of water with 10 min continuous stirring. Aniline (100 μ L, 1.02 g/cm³, 1.1 mmol) at 25 °C was added and stirred for additional 1h. After cooling the mixture at 10 °C, an aqueous solution of APS was added dropwise to the reaction mixture that was allowed to stand at 5 °C temperature for 18h. The resulting deep-green precipitate was washed with water followed by methanol several times to remove the oligomers and excess APS from the reaction mixture. Finally, the product was dried under vacuum to get high-aspect-ratio BTCA-doped PANI (BDP) fibers.

Preparation of BDP@Ag Composite. A 100 mg amount of BDP fiber was dispersed in 10 mL of Milli-Q water in a culture tube equipped with magnetic stirrer at room temperature (25 °C). A 10 mL amount of AgNO₃ solution (10⁻²/10⁻³/10⁻⁴ M) was added dropwise, and the resulting mixture was stirred for 2–3h (Table S1). Finally, BDP@Ag composites were collected by centrifugation at 10 000 rpm and washed with water several times to remove unreacted AgNO₃ from the surface of BDP fibers.

SERS Measurements. 4-MBA and R6G were each used as an analyte molecule, and SERS active substrates were prepared from small amount of BDP@Ag composites (dispersed in ethanol or water) stirred with different concentrations (\sim 10⁻⁵–10⁻¹⁰ M) of above-mentioned analyte molecules. The resulting mixture was spotted on a coverslip and dried under N₂ atmosphere prior to SERS measurements. Samples were scanned with 514.5 nm laser, 10 s accumulation times with two scans by using a 50 \times microscopic lens with laser intensity = 7 μ W.

Catalytic Reduction of 4-NTP. Reduction of 4-NTP was monitored by SERS method. Typically, 100 μ L of a yellow ethanol solution of 4-NTP (1 mM) was poured into a quartz cell (1 cm path length) containing 2 mL of water. Subsequently, BDP@Ag composite (\sim 0.3 wt %) and 100 μ L of ice-cold NaBH₄ solution (3 mM) were added to the quartz cell that was subjected to SERS measurement at different times to monitor the reduction process.^{30–32}

RESULTS AND DISCUSSION

Morphology of BDP@Ag Composites. TEM micrographs (Figure 1) of the synthesized BDP@Ag composites show that BDP fibers remain fibrillar in shape after the reaction with AgNO₃ solution and that Ag NPs are homogeneously dispersed onto the BDP fiber for all compositions. The population of Ag NPs on BDP fiber is tunable by controlling AgNO₃ concentration, and maximum coverage of Ag NP is obtained for BDP@Ag1.0. However, the size of Ag NP on BDP fiber remains unaffected by the concentration. At higher concentrations of AgNO₃ (in BDP@Ag10), dendrite-like Ag nanostructures (Figure 1b) were seen outside the fiber surface, along with few spherical Ag NPs on the BDP surface (inset of Figure 1a). Dendrite shapes are significantly reduced at lower concentrations of AgNO₃ (Figure 1d–i). In high magnification of TEM images, spherical Ag NPs (\sim 10 nm diameter) are clearly visible and are systematically arranged by an in situ technique over the surface of BDP fiber. It suggests the compact contact between the Ag NPs and surface of BDP fiber. The weight percent of Ag present in the system (on BDP surface and outside) estimated by ICP-AES measurement is 48.95, 34.6, and 11.8 wt % for BDP@Ag10, BDP@Ag1.0, and BDP@Ag0.1, respectively. Careful observation of dark-field images (Figure 1c,f,i) provides interesting information on the loading density of Ag NPs on BDP fibers, and the higher density of Ag NPs is observed on BDP@Ag1.0. The loading density of Ag NPs, the fibrillar morphology of BDP fiber, and

the spherical shape of Ag NPs of BDP@Ag composites are confirmed by TEM studies.

A typical HRTEM image (Figure 2a) shows the spherical shape of Ag NPs with diameter \sim 10 nm. From FFT images

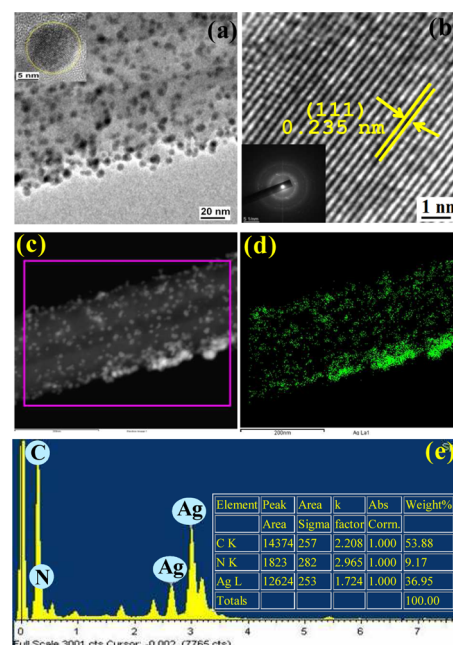


Figure 2. (a) HRTEM image of BDP@Ag1.0 composite, inset image represents single spherical-shaped Ag nanoparticle (Ag NP); (b) FFT image of Ag NPs with SAED pattern (inset image); (c) dark-field image of BDP@Ag1.0 composite; (d) corresponding mapping image of BDP@Ag1.0 composite; and (e) EDX pattern of BDP@Ag1.0 composite.

(Figure 2b), the estimated lattice distance is 0.235 nm, which exactly matches the (111) plane of Ag NPs in XRD (Figure 3)

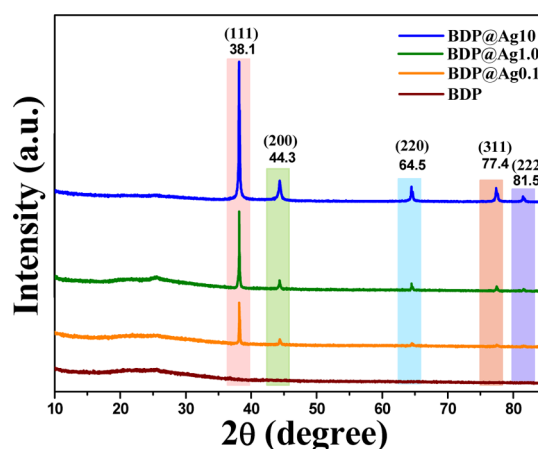


Figure 3. XRD pattern of BDP@Ag composites synthesized at room temperature.

and selected-area electron diffraction (SAED; inset, Figure 2b). Ag NPs are fully decorated on BDP fiber uniformly in BDP@Ag1.0 composite (Figure 1d–f). The EDX pattern (Figure 2e) of BDP@Ag1.0 composite indicates the presence of carbon, oxygen, nitrogen, and silver. Dendrite-like Ag-nano morphology that was formed at higher concentrations of AgNO₃ (in BDP@Ag10 composite) is further ascertained by mapping images

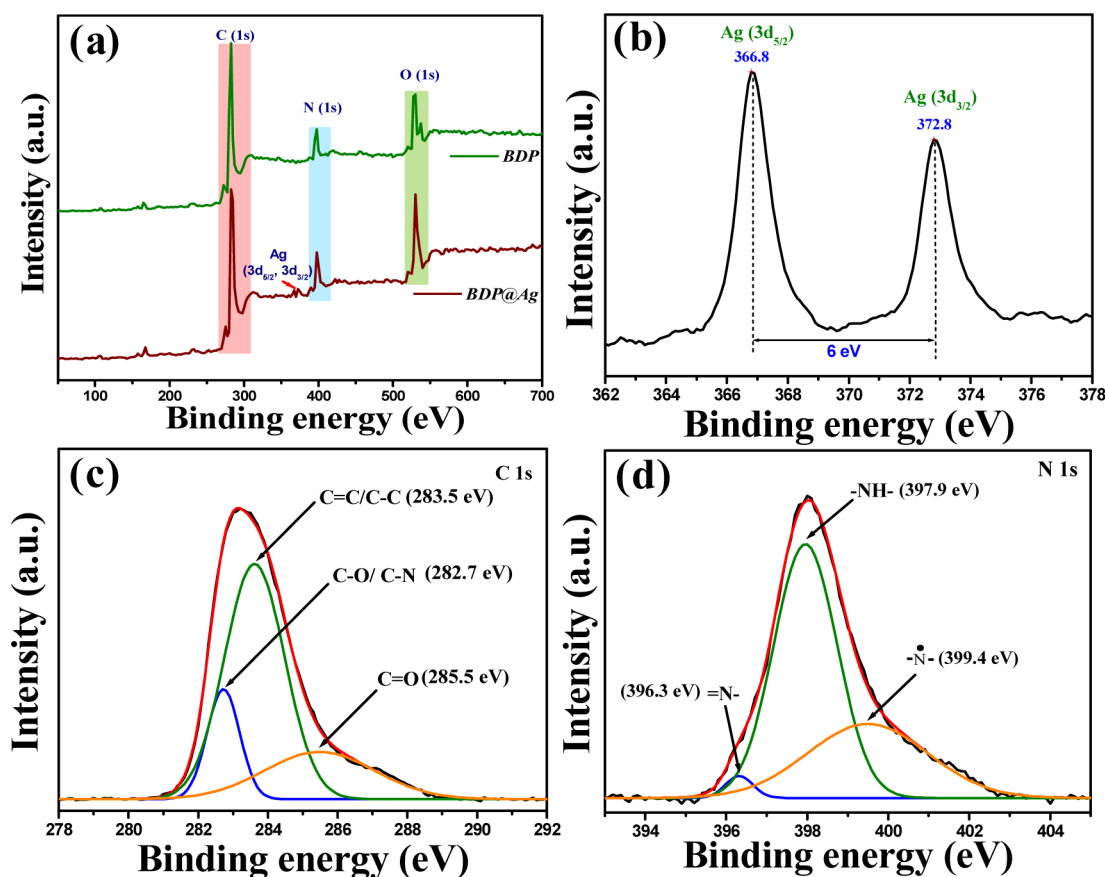


Figure 4. XPS spectra of BDP@Ag1.0 composite: (a) full scan and enlarged spectra of (b) Ag, (c) carbon, and (d) nitrogen.

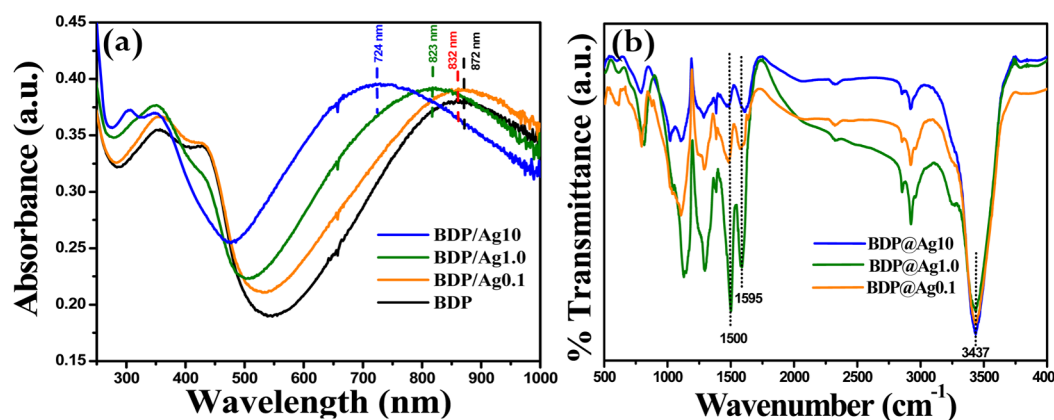


Figure 5. (a) UV-vis spectra of BDP@Ag composites, (b) FTIR spectra of BDP@Ag composites synthesized at room temperature.

(Figure S9). Spherelike Ag NPs were formed in BDP@Ag1.0 and BDP@Ag0.1 composites.

XRD Study. XRD patterns of BDP@Ag composites (Figure 3) reveal the presence of amorphous PANI with crystalline Ag NPs. A broad peak centered at $2\theta = 25^\circ$ is indicative of the amorphous nature of PANI, and five sharp peaks at range $2\theta \approx 38\text{--}82^\circ$ are for crystalline nature of Ag NPs. The crystalline peaks centered at $2\theta \approx 38.1, 44.3, 64.5, 77.4,$ and 82.5° correspond to the (111), (200), (220), and (311) crystal planes of the face-centered cubic structure of Ag NPs. This result indicates that tiny Ag NPs were embedded in PANI matrix.^{42,43} Layer distance between two similar crystal planes of Ag NP has been calculated from Bragg's equations: $n\lambda = 2d \sin \theta$, where λ is the X-ray wavelength (0.154 nm), d is the separation between

two similar crystal planes, and θ is the Bragg angle (in degree). Here, the calculated layer distance for the (111) crystal plane by using Bragg's equation is 0.235 nm. The peak intensity of crystalline Ag NP gradually decreases with decreasing the amount of silver present in the system.⁴⁴

XPS Study. Furthermore, we explore X-ray photoelectron spectroscopy (XPS) of BDP@Ag1.0 composite (Figure 4a) in the region of binding energy (E_b) = 50–700 eV to study the formation of Ag NP. In the region of $E_b = 362\text{--}378$ eV (Figure 4b), XPS signals at ~ 366.8 and 372.8 eV correspond to Ag $3d_{5/2}$ and Ag $3d_{3/2}$ energy levels, respectively.^{45–47} Other strong XPS signals at 282.5, 397.5, and 530 eV are assigned to C 1s, N 1s, and O 1s, respectively (Figures 2c,d and S2), indicating the chemical environment of C, N, and O due to PANI.^{48,49} Peak

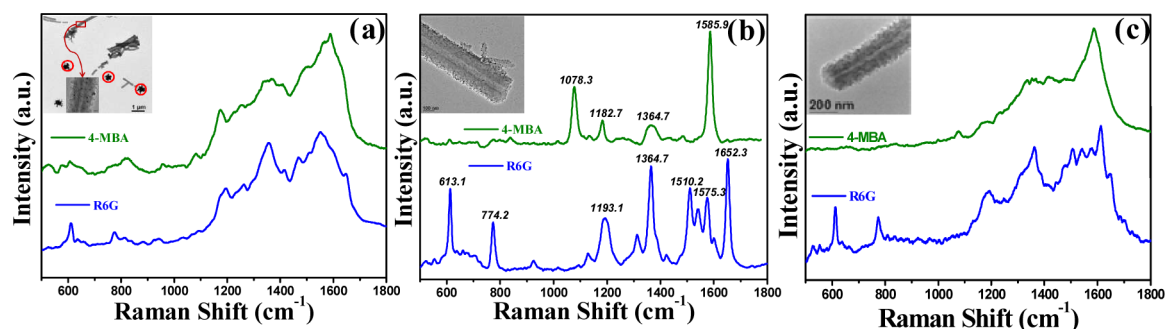


Figure 6. SERS spectra of 4-MBA and R6G produced by substrates (a) BDP@Ag10 (inset, TEM image), (b) BDP@Ag1.0 (inset, TEM image), and (c) BDP@Ag0.1 (inset, TEM image).

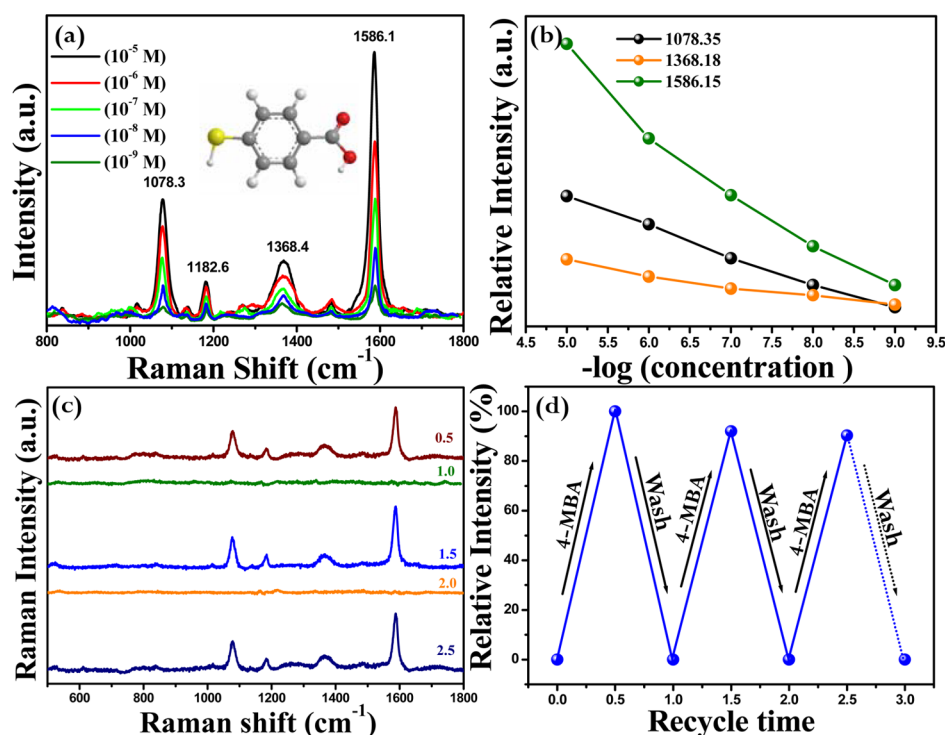


Figure 7. (a) Concentration-dependent SERS spectra of 4-MBA excited with 514.5 nm laser with BDP@Ag1.0 as an active substrate; inset, molecular structure of 4-MBA. (b) Changing of SERS intensity vs logarithm of analyte concentration. (c) Raman spectra acquired from BDP@Ag1.0 with three repeated loadings of 4-MBA (1×10^{-5} M) and two repeated washes with ethanol. (d) SERS responses (Raman peak centered at 1586.1 cm^{-1}) of BDP@Ag1.0 with 4-MBA and after ethanol wash.

positions of Ag $3d_{5/2}$ and $3d_{3/2}$ are slightly shifted from literature values, but peak difference is same (6 eV) as literature.⁵⁰

UV-Vis and FTIR Study. UV-vis investigations show three characteristic absorption peaks centered at 365, 450, and 930 nm (Figure 5a). The peak at 365 nm is ascribed to the $\pi-\pi^*$ transition of the benzenoid rings; another two peaks at 450 and 830 nm are attributed to the polaron- π^* transition and the π -polaron transition, respectively.^{39-41,51} The π -polaron peak is red-shifted with increasing Ag concentration in the composite. After addition of Ag ion to BDP fiber, the radical of polaron form of PANI reduces Ag ions to Ag(0), leading to the formation of Ag NPs, and the corresponding band gap of π -polaron state of PANI increases as is reflected on EPR and $I-V$ data (Figures S2 and S3). Characteristic absorption of Ag NP at ~ 410 nm is not resolved in the spectra because it is probably overlapped with that of the broad $\pi-\pi^*$ and the polaron- π^* band of PANI.

The stretching vibrations at 815, 1130, 1297, 1500, 1595, and 3430 cm^{-1} (Figure 5b) prove the presence of emeraldine salt state of PANI in our synthesized composites. The characteristic stretching vibration bands at 815 and 1130 cm^{-1} are for $\gamma\text{C-H}$ aromatic in-plane and out-of-plane deformation of 1,4-disubstituted benzene; the stretching vibration band at 1297 cm^{-1} is for $\gamma\text{C-N}$ of the secondary aromatic amine. Another two stretching vibration bands are at 1500 cm^{-1} (for $\gamma\text{C=C}$ for benzenoid rings) and 1595 cm^{-1} (for $\gamma\text{C=C}$ quinoid rings). The band at ~ 3430 cm^{-1} is for the N-H stretching vibration for PANI.³⁹⁻⁴¹

The TGA curves of BDP and BDP@Ag composite (Figure S4) show three-step weight-loss behavior. The weight loss at ~ 100 $^{\circ}\text{C}$ indicates some amount of moisture or solvent present in the samples. Another weight loss at ~ 290 $^{\circ}\text{C}$ is for dedoping and decomposition of BTCA dopant; the last step of degradation at ~ 500 $^{\circ}\text{C}$ is for decomposition of PANI chain.^{39,52-54}

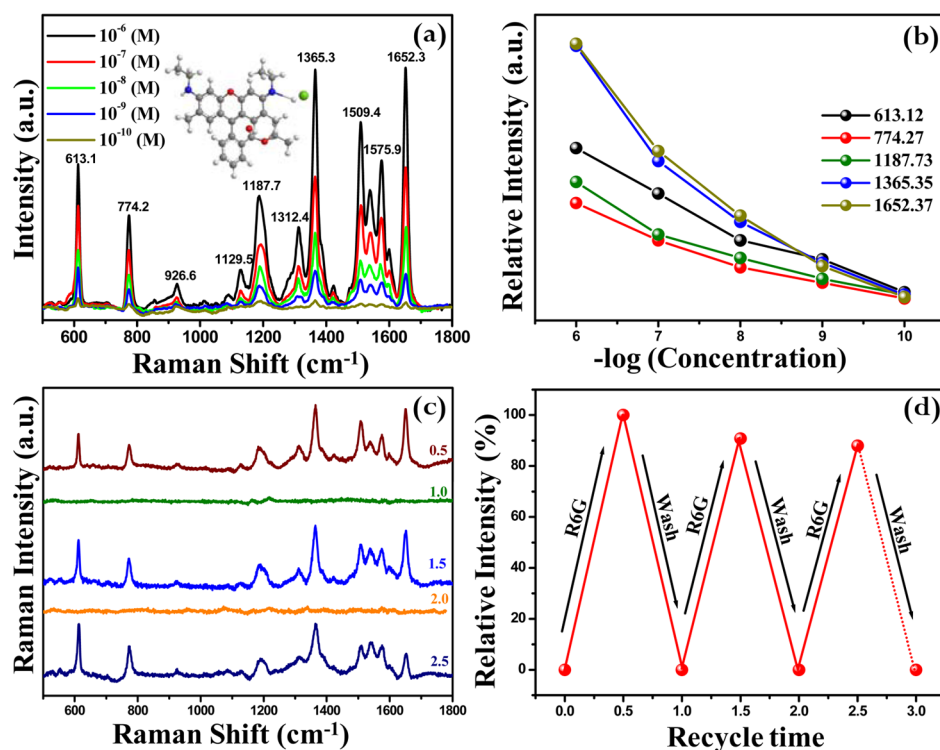


Figure 8. (a) Concentration-dependent SERS spectra of R6G with BDP@Ag1.0 as an active SERS substrate; inset, molecular structure for R6G. (b) Changing of SERS intensity vs log of analyte concentration. (c) Raman spectra recorded from the BDP@Ag1.0 with three repeated loadings of R6G (1×10^{-6} M) and two repeated washes with water. (d) SERS responses (Raman peak centered at 1365.3 cm^{-1}) of BDP@Ag1.0 with R6G and after washing with water.

BDP@Ag Composite as a Sensitive SERS Substrate. To evaluate the SERS activity, BDP@Ag composites (substrate) are dispersed in either an ethanolic solution of 4-MBA or an aqueous solution of R6G. Depending upon the population density of Ag NPs on BDP fiber, surface enhancement changes from BDP@Ag10 to BDP@Ag0.1 (Figure 6). Among three BDP@Ag composites, BDP@Ag1.0 composite shows excellent surface enhancement (Figure 6b) that can be attributed to the higher effective surface area of Ag NPs, which is higher than that of two other composites. The other two composites (BDP@Ag10 and BDP@Ag0.1) show nominal surface enhancement (Figure 6a,c) because of the larger Ag-clusterlike morphology of BDP@Ag10 that reduces the effective surface area on the metallic surface. Very low SERS activity is expected from BDP@Ag0.1 because of the lower percentage of Ag NPs on BDP fibers, though the particles are the same in size and spherical in shape. Apart from the three above-mentioned BDP@Ag composites, four additional composites (BDP@Ag4.0, BDP@Ag2.0, BDP@Ag0.7, and BDP@Ag0.3) depending on the molar concentration of AgNO_3 have been prepared (Supporting Information, Figure S10). On the basis of HRTEM studies and SERS results, BDP@Ag1.0 has been picked up for the detection of analyte molecules.

SERS Study of 4-MBA. SERS spectra of 4-MBA at different molar concentrations (10^{-5} – 10^{-9} M, Figure 7) produce two strong signals at ~ 1586.1 and 1078.3 cm^{-1} that correspond to characteristic aromatic ring vibrations. Two other weak signals at ~ 1151 and 1182.6 cm^{-1} are for C–H deformation modes.⁵⁵ All four peaks (1078.3 , 1182.6 , 1368.4 , and 1586.1 cm^{-1}) have experienced superior enhancement in the presence of BDP@Ag1.0 composite compared to those in the normal Raman spectra (NRS) for 4-MBA (Figure S6), and the analytical

enhancement factor (AEF) for the more-intense peak (1586.1 cm^{-1}) is 1.9×10^8 . In the plot of intensity versus $-\log(\text{concentration})$, the peak intensity of 4-MBA is gradually reduced with lowering of the analyte concentration (Figure 7b). Well-resolved Raman spectra are limpidly observed at nanomolar concentration of 4-MBA in the presence of BDP@Ag1.0 composite as a SERS substrate.

SERS Study for R6G. SERS spectra of R6G (10^{-6} – 10^{-10} M, Figure 8) reveal several well-resolved Raman signals at 613.1 cm^{-1} (C–C–C in-plane bending), 774.2 cm^{-1} (C–H out-of-plane bending), 1187.7 cm^{-1} (C–H in-plane bending), and 1312.4 cm^{-1} (C–O–C stretching), and C–C stretching modes for aromatic rings show peaks at 1365.3 , 1509.4 , 1575.9 , and 1652.3 cm^{-1} .^{56,57} Slight Raman shift that has been shown in spectra is due to the weak interaction between the analyte molecule and the BDP@Ag substrate. The plot of intensity versus $-\log(\text{concentration})$ (Figure 8b) shows the gradual decrease of intensity with lowering of the analyte concentration. Similarly, here all peaks have experienced surface enhancement in the presence of BDP@Ag1.0 composite compared to those of NRS of R6G (Figure S7). Raman spectra are clearly noticed below nanomolar concentration of R6G in the presence of BDP@Ag1.0 composite. The calculated analytical enhancement factor (AEF) is 1.2×10^9 .

To demonstrate the recyclability property for the real application, three cycles were performed by successive SERS measurement and washing. Raman spectra (Figures 7c and 8c) of each cycle are similar to each other, and analyte molecules can be completely removed by rinsing the substrate with solvent. By considering the intensity of the peak at 1586.1 cm^{-1} (4-MBA) and 1365.3 cm^{-1} (R6G), good reproducibility (Figures 7d and 8d) is achieved with BDP@Ag1.0 composite

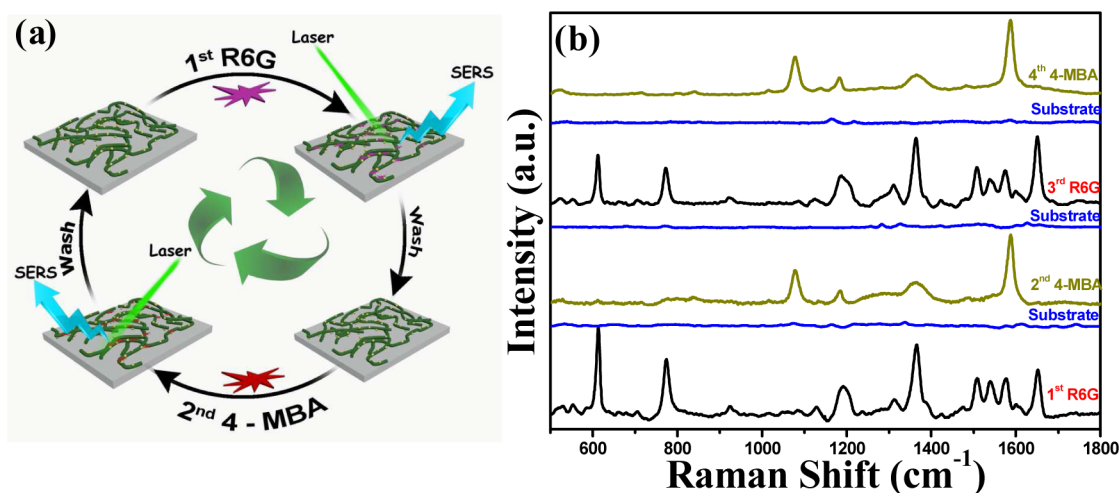


Figure 9. (a) Schematic recyclability representation of BDP@Ag substrate and (b) the corresponding SERS spectra of recycle detection process.

for each case. These results indicate the suitability as well as reusability of BDP@Ag1.0 as a recyclable SERS substrate for the detection of individual analyte molecules down to nanomolar concentration.

Recyclability of SERS Substrate with a Different Analyte. Another important issue is the recyclability of BDP@Ag as SERS substrate with different analyte molecules. In Figure 9, the strong SERS signals are also observed with R6G and 4-MBA used consecutively. The recyclable behavior of BDP@Ag1.0 composite with several analyte molecules is much more interesting than that with a single molecule over several times. An important outcome of the observation is that the recyclability of BDP@Ag1.0 as SERS substrate reproduces strong signals.

Reduction of 4-Nitrothiophenol Monitored by SERS Study. Furthermore, catalytic activity of BDP@Ag1.0 composite has been explored by selecting 4-NTP as an analyte molecule. SERS spectra at different times (Figure 10) reveal the gradual reduction reaction of 4-NTP by BDP@Ag1.0 composite. A gradual decrease of the NO_2 stretching bands at 1573 and 1393 cm^{-1} have been observed and completely

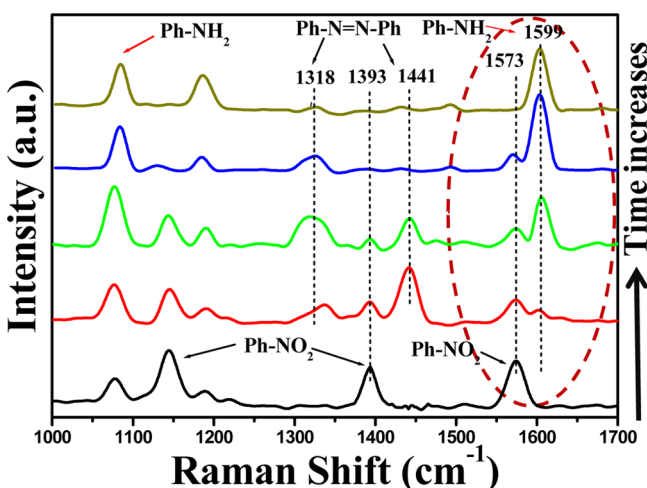


Figure 10. SERS spectra for reduction of 4-NTP recorded in the presence of BDP@Ag1.0 as a SERS substrate cum catalyst with different times. From bottom to top, time increases (0, 120, 240, 360, and 480 s) after addition of NaBH_4 solution.

disappeared after 480 s, implying that the NO_2 group of 4-NTP is fully reduced. A new band emerges at 1599 cm^{-1} , which is assigned to the amino vibrational mode of 4-aminothiophenol (4-ATP).^{58,59} Quantitative calculation of the concentration of 4-NTP and 4-ATP at different times have been performed by comparing two characteristic peak intensity (1573 and 1599 cm^{-1}) of 4-NTP and 4-ATP, respectively. The plot of $\ln(C_t/C_0)$ vs time gives rate of reaction, where C_t and C_0 are the concentration of 4-NTP at time t and 0 s, respectively. The linear relationship of the plot $\ln(C_t/C_0)$ versus time implies that reaction follows pseudo-first-order kinetics, assuming the concentration of NaBH_4 is much higher compared to the concentration of 4-NTP. The slope of the linear plot provides the rate of reaction ($3.23 \times 10^{-3} \text{ s}^{-1}$, Figure S8). In SERS spectra, characteristic peaks at 1318 and 1441 cm^{-1} are assigned to 4,4'-dimercaptoazobenzene (Ph-N=N-Ph), an intermediate formed during the reduction reaction that is further proved by UV-vis studies (Figure S4). The peak at 411 nm for the 4-nitrothiophenolate ion (from treatment of 4-NTP with NaBH_4) is gradually diminished, and subsequently, the 4-ATP peak at 268 nm is enhanced. Assuming pseudo-first-order kinetics, the estimated rate of the reaction from UV-vis study is $3.88 \times 10^{-3} \text{ s}^{-1}$, which is very near to that obtained by SERS study (Figure S8).

CONCLUSIONS

In the present manuscript, we have successfully decorated spherical-shaped Ag NPs over a PANI nanofiber by a simple solution-dipping method at room temperature where BDP fiber acts both as a reducer and a stabilizer. The shape and loading density of Ag NPs on the BDP surface depends on AgNO_3 molar concentration with respect to PANI. Prepared BDP@Ag composites behave as very sensitive SERS substrates for detection of 4-MBA and R6G down to nanomolar concentration with excellent recyclability. An important accomplishment is achieving the function of BDP@Ag composite as a SERS substrate and reduction catalyst simultaneously.

ASSOCIATED CONTENT

Supporting Information

Preparation of BDP@Ag composites (Table S1); XPS spectra of O 1s in BDP@Ag1.0 composite; EPR study of BDP@Ag composites; current-voltage study of BDP@Ag composites;

TG analysis; UV–vis spectra of 4-NTP reduction; AEF calculation for 4-MBA and R6G. The Supporting Information is available free of charge on the ACS Publications website at DOI: 10.1021/acsami.5b01806.

AUTHOR INFORMATION

Corresponding Author

*E-mail: psum2@iacs.res.in.

Notes

The authors declare no competing financial interest.

ACKNOWLEDGMENTS

Dr. Malik acknowledges CSIR, INDIA (project no. 02(0161)/13/EMR-II) for the financial support. S.M. is thankful to CSIR, New Delhi, India for the fellowship. The authors are thankful to the Unit of Nanoscience (DST, Government of India) at IACS, Kolkata, for FEGTEM and XPS.

REFERENCES

- (1) Nie, S.; Emory, S. R. Probing Single Molecules and Single Nanoparticles by Surface-Enhanced Raman Scattering. *Science* **1997**, *275*, 1102–1106.
- (2) Kodiyath, R.; Wang, J.; Combs, Z. A.; Chang, S.; Gupta, M. K.; Anderson, K. D.; Brown, R. J. C.; Tsukruk, V. V. SERS Effects in Silver-Decorated Cylindrical Nanopores. *Small* **2011**, *7*, 3452–3457.
- (3) Kleinman, S. L.; Ringe, E.; Valley, N.; Wustholz, K. L.; Phillips, E.; Scheidt, K. A.; Schatz, G. C.; Duyne, R. P. V. Single-Molecule Surface-Enhanced Raman Spectroscopy of Crystal Violet Isotopologues: Theory and Experiment. *J. Am. Chem. Soc.* **2011**, *133*, 4115–4122.
- (4) Saha, K.; Agasti, S. S.; Kim, C.; Li, X.; Rotello, V. M. Gold Nanoparticles in Chemical and Biological Sensing. *Chem. Rev.* **2012**, *112*, 2739–2779.
- (5) Fu, K.; Li, S.; Jiang, X.; Wang, Y.; Willis, B. G. DNA Gold Nanoparticle Nanocomposite Films for Chemiresistive Vapor Sensing. *Langmuir* **2013**, *29*, 14335–14343.
- (6) Zhou, X.; Xu, W.; Wang, Y.; Kuang, Q.; Shi, Y.; Zhong, L.; Zhang, Q. Fabrication of Cluster/Shell Fe₃O₄/Au Nanoparticles and Application in Protein Detection via a SERS Method. *J. Phys. Chem. C* **2010**, *114*, 19607–19613.
- (7) Ditto, A. J.; Shah, K. N.; Robishaw, N. K.; Panzner, M. J.; Youngs, W. J.; Yun, Y. H. The Interactions between L-Tyrosine Based Nanoparticles Decorated with Folic Acid and Cervical Cancer Cells under Physiological Flow. *Mol. Pharmaceutics* **2012**, *9*, 3089–3098.
- (8) Zhang, H.; Jin, M.; Xia, Y. Enhancing the Catalytic and Electrocatalytic Properties of Pt-based Catalysts by forming Bimetallic Nanocrystals with Pd. *Chem. Soc. Rev.* **2012**, *41*, 8035–8049.
- (9) Zhou, Y.; Cheng, X.; Du, D.; Yang, J.; Zhao, N.; Ma, S.; Zhong, T.; Lin, Y. Graphene–Silver Nanohybrids for Ultrasensitive Surface Enhanced Raman Spectroscopy: Size Dependence of Silver Nanoparticles. *J. Mater. Chem. C* **2014**, *2*, 6850–6858.
- (10) Baker, C. O.; Shedd, B.; Tseng, R. J.; Martinez-Morales, A.; Ozkan, C. S.; Ozkan, M.; Yang, Y.; Kaner, R. B. Size Control of Gold Nanoparticles Grown on Polyaniline Nanofibers for Bistable Memory Devices. *ACS Nano* **2011**, *5*, 3469–3474.
- (11) Tseng, R. J.; Huang, J.; Ouyang, J.; Kaner, R. B.; Yang, Y. Polyaniline Nanofiber/Gold Nanoparticle Nonvolatile Memory. *Nano Lett.* **2005**, *5*, 1077–1080.
- (12) Li, X. Z.; Wu, K. L.; Yea, Y.; Wei, X. W. Gas-Assisted Growth of Boron-Doped Nickel Nanotube Arrays: Rapid Synthesis, Growth Mechanisms, Tunable Magnetic Properties, and Super-Efficient Reduction of 4-Nitrophenol. *Nanoscale* **2013**, *5*, 3648–3653.
- (13) An, Q.; Yu, M.; Zhang, Y.; Ma, W.; Guo, J.; Wang, C. Fe₃O₄@Carbon Microsphere Supported Ag–Au Bimetallic Nanocrystals with the Enhanced Catalytic Activity and Selectivity for the Reduction of Nitroaromatic Compounds. *J. Phys. Chem. C* **2012**, *116*, 22432–22440.
- (14) Xu, P.; Han, X.; Zhang, B.; Du, Y.; Wang, H. L. Multifunctional Polymer–Metal Nanocomposites via Direct Chemical Reduction by Conjugated Polymers. *Chem. Soc. Rev.* **2014**, *43*, 1349–1360.
- (15) Kleinman, S. L.; Ringe, E.; Valley, N.; Wustholz, K. L.; Phillips, E.; Scheidt, K. A.; Schatz, G. C.; Duyne, R. P. V. Single-Molecule Surface-Enhanced Raman Spectroscopy of Crystal Violet Isotopologues: Theory and Experiment. *J. Am. Chem. Soc.* **2011**, *133*, 4115–4122.
- (16) Auguie, B.; Gomez, J. L. A.; Martinez, A. G.; Marzan, L. M. L. Fingers Crossed: Optical Activity of a Chiral Dimer of Plasmonic Nanorods. *J. Phys. Chem. Lett.* **2011**, *2*, 846–851.
- (17) Liu, W.; Zhu, Z.; Deng, K.; Li, Z.; Zhou, Y.; Qiu, H.; Gao, Y.; Che, S.; Tang, Z. Gold Nanorod@Chiral Mesoporous Silica Core–shell Nanoparticles with Unique Optical Properties. *J. Am. Chem. Soc.* **2013**, *135*, 9659–9664.
- (18) Zhu, Z.; Meng, H.; Liu, W.; Liu, X.; Gong, J.; Qiu, X.; Jiang, L.; Wang, D.; Tang, Z. Superstructures and SERS Properties of Gold Nanocrystals with Different Shapes. *Angew. Chem., Int. Ed.* **2011**, *50*, 1593–1596.
- (19) He, H.; Cai, W.; Lin, Y.; Chen, B. Au Nanochain-Built 3D Netlike Porous Films based on Laser Ablation in water and Electrophoretic Deposition. *Chem. Commun.* **2010**, *46*, 7223–7225.
- (20) Tessier, P. M.; Velev, O. D.; Kalambur, A. T.; Rabolt, J. F.; Lenhoff, A. M.; Kaler, E. W. Assembly of Gold Nanostructured Films Templated by Colloidal Crystals and Use in Surface-Enhanced Raman Spectroscopy. *J. Am. Chem. Soc.* **2000**, *122*, 9554–9555.
- (21) Lee, C. H.; Tian, L.; Singamaneni, S. Paper-Based SERS Swab for Rapid Trace Detection on Real-World Surfaces. *ACS Appl. Mater. Interfaces* **2010**, *2*, 3429–3435.
- (22) Gupta, M. K.; Chang, S.; Singamaneni, S.; Drummy, L. F.; Gunawidjaja, R.; Naik, R. R.; Tsukruk, V. V. pH-Triggered SERS via Modulated Plasmonic Coupling in Individual Bimetallic Nanocobs. *Small* **2011**, *7*, 1192–1198.
- (23) Chang, S.; Ko, H.; Singamaneni, S.; Gunawidjaja, R.; Tsukruk, V. V. Nanoporous membranes with Mixed Nanoclusters for Raman-Based Label-Free Monitoring of Peroxide Compounds. *Anal. Chem.* **2009**, *81*, 5740–5748.
- (24) Yan, J.; Han, X.; He, J.; Kang, L.; Zhang, B.; Du, Y.; Zhao, H.; Dong, C.; Wang, H. L.; Xu, P. Highly Sensitive Surface-Enhanced Raman Spectroscopy (SERS) Platforms Based on Silver Nanostructures Fabricated on Polyaniline Membrane Surfaces. *ACS Appl. Mater. Interfaces* **2012**, *4*, 2752–2756.
- (25) Xu, P.; Mack, N. H.; Jeon, S. H.; Doorn, S. K.; Han, X.; Wang, H. L. Facile Fabrication of Homogeneous 3D Silver Nanostructures on Gold-Supported Polyaniline Membranes as Promising SERS Substrates. *Langmuir* **2010**, *26*, 8882–8886.
- (26) Zhao, Y.; Sun, L.; Xi, M.; Feng, Q.; Jiang, C.; Fong, H. Electrospun TiO₂ Nanofelt Surface-Decorated with Ag Nanoparticles as Sensitive and UV-Cleanable Substrate for Surface Enhanced Raman Scattering. *ACS Appl. Mater. Interfaces* **2014**, *6*, 5759–5767.
- (27) Wang, W.; Yin, Y.; Tan, Z.; Liu, J. Coffee-Ring Effect-based Simultaneous SERS Substrate Fabrication and Analyte Enrichment for Trace Analysis. *Nanoscale* **2014**, *6*, 9588–9593.
- (28) Xie, W.; Schlucker, S. Medical Applications of Surface-Enhanced Raman Scattering. *Phys. Chem. Chem. Phys.* **2013**, *15*, 5329–5344.
- (29) Zhang, B.; Xu, P.; Xie, X.; Wei, H.; Li, Z.; Mack, N. H.; Han, X.; Xu, H.; Wang, H. L. Acid-Directed Synthesis of SERS-Active Hierarchical Assemblies of Silver Nanostructures. *J. Mater. Chem.* **2011**, *21*, 2495–2501.
- (30) Cui, Q.; Yashchenok, A.; Zhang, L.; Li, L.; Masic, A.; Wienskol, G.; Mohwald, H.; Bargheer, M. Fabrication of Bifunctional Gold/Gelatin Hybrid Nanocomposites and Their Application. *ACS Appl. Mater. Interfaces* **2014**, *6*, 1999–2002.
- (31) Kang, L.; Xu, P.; Zhang, B.; Tsai, H.; Han, X.; Wang, H. L. Laser Wavelength- and Power-Dependent Plasmon-Driven Chemical Reactions Monitored using Single Particle Surface Enhanced Raman Spectroscopy. *Chem. Commun.* **2013**, *49*, 3389–3391.
- (32) Kang, L.; Xu, P.; Chen, D.; Zhang, B.; Du, Y.; Han, X.; Li, Q.; Wang, H. L. Amino Acid-Assisted Synthesis of Hierarchical Silver

Microspheres for Single Particle Surface-Enhanced Raman Spectroscopy. *J. Phys. Chem. C* **2013**, *117*, 10007–10012.

(33) Zhao, L. B.; Zhang, M.; Huang, Y. F.; Williams, C. T.; Wu, D. Y.; Ren, B.; Tian, Z. Q. Theoretical Study of Plasmon-Enhanced Surface Catalytic Coupling Reactions of Aromatic Amines and Nitro Compounds. *J. Phys. Chem. Lett.* **2014**, *5*, 1259–1266.

(34) Tang, X.; Cai, W.; Yang, L.; Liu, J. Monitoring Plasmon-Driven Surface Catalyzed Reactions in situ using Time-Dependent Surface Enhanced Raman Spectroscopy on Single Particles of Hierarchical Peony-like Silver Microflowers. *Nanoscale* **2014**, *6*, 8612–8616.

(35) Mondal, S.; Rana, U.; Bhattacharjee, R. R.; Malik, S. One Pot Green Synthesis of Polyaniline coated Gold Nanorods and its Applications. *RSC Adv.* **2014**, *4*, 57282–57289.

(36) Wunder, S.; Polzer, F.; Lu, Y.; Mei, Y.; Ballauff, M. Kinetic Analysis of Catalytic Reduction of 4-Nitrophenol by Metallic Nanoparticles Immobilized in Spherical Polyelectrolyte Brushes. *J. Phys. Chem. C* **2010**, *114*, 8814–8820.

(37) Kolla, H. S.; Surwade, S. P.; Zhang, X.; MacDiarmid, A. G.; Manohar, S. K. Absolute Molecular Weight of Polyaniline. *J. Am. Chem. Soc.* **2005**, *127*, 16770–16777.

(38) Li, D.; Huang, J.; Kaner, R. B. Polyaniline Nanofibers: A Unique Polymer Nanostructure for Versatile Applications. *Acc. Chem. Res.* **2009**, *42*, 135–145.

(39) Rana, U.; Chakrabarti, K.; Malik, S. Benzene Tetracarboxylic Acid Doped Polyaniline Nanostructures: Morphological, Spectroscopic and Electrical Characterization. *J. Mater. Chem.* **2012**, *22*, 15665–15671.

(40) Rana, U.; Malik, S. Graphene Oxide/Polyaniline Nanostructures: Transformation of 2D Sheet to 1D Nanotube and in situ Reduction. *Chem. Commun.* **2012**, *48*, 10862–10864.

(41) Rana, U.; Chakrabarti, K.; Malik, S. *In situ* Preparation of Fluorescent Polyaniline Nanotubes Doped with Perylene Tetracarboxylic Acids. *J. Mater. Chem.* **2011**, *21*, 11098–11100.

(42) Drury, A.; Chaure, S.; Kroll, M.; Nicolosi, V.; Chaure, N.; Blau, W. J. Fabrication and Characterization of Silver/Polyaniline Composite Nanowires in Porous Anodic Alumina. *Chem. Mater.* **2007**, *19*, 4252–4258.

(43) Pillalamarri, S. K.; Blum, F. D.; Tokuhiko, A. T.; Bertino, M. F. One-Pot Synthesis of Polyaniline–Metal Nanocomposites. *Chem. Mater.* **2005**, *17*, 5941–5944.

(44) Patel, A. C.; Li, S.; Wang, C.; Zhang, W.; Wei, Y. Electrospinning of Porous Silica Nanofibers Containing Silver Nanoparticles for Catalytic Applications. *Chem. Mater.* **2007**, *19*, 1231–1238.

(45) Moholkar, A. V.; Kim, J. H.; Kalubarme, R. S.; Park, C. J.; Patil, P. S. Gold Nanoparticles Prepared by Glycinate Ionic Liquid Assisted Multi-Photon Photoreduction. *Phys. Chem. Chem. Phys.* **2012**, *14*, 11930–11936.

(46) Kang, S. Y.; Kim, K. Comparative Study of Dodecanethiol-Derivatized Silver Nanoparticles Prepared in One-Phase and Two-Phase Systems. *Langmuir* **1998**, *14*, 226–230.

(47) Gao, Y.; Shan, D.; Cao, F.; Gong, J.; Li, X.; Ma, H.; Su, Z.; Qu, L. Silver/Polyaniline Composite Nanotubes: One-Step Synthesis and Electrocatalytic Activity for Neurotransmitter Dopamine. *J. Phys. Chem. C* **2009**, *113*, 15175–15181.

(48) Tsunoyama, H.; Sakurai, H.; Ichikuni, N.; Negishi, Y.; Tsukuda, T. Colloidal Gold Nanoparticles as Catalyst for Carbon-Carbon Bond Formation: Application to Aerobic Homocoupling of Phenylboronic Acid in Water. *Langmuir* **2004**, *20*, 11293–11296.

(49) Li, X. R.; Li, X. L.; Xu, M. C.; Xu, J. J.; Chen, H. Y. Gold Nanodendrites on Graphene Oxide Nanosheets for Oxygen Reduction Reaction. *J. Mater. Chem. A* **2014**, *2*, 1697–1803.

(50) Wagner, C. D.; Riggs, W. M.; Davis, C. E.; Moulder, J. F. *Handbook of X-ray Photoelectron Spectroscopy*; Muilenberg, G. E., Ed.; PerkinElmer Corporation: Eden Prairie, MN, 1979; p 122.

(51) Rana, U.; Mondal, S.; Sannigrahi, J.; Sukul, P. K.; Amin, Md. A.; Majumdar, S.; Malik, S. Aromatic Bi-, Tri- and Tetracarboxylic Acid Doped Polyaniline Nanotubes: Effect on Morphologies and Electrical Transport Properties. *J. Mater. Chem. C* **2014**, *2*, 3382–3389.

(52) Zhang, L.; Long, Y.; Chen, Z.; Wan, M. The Effect of Hydrogen Bonding on Self-Assembled Polyaniline Nanostructures. *Adv. Funct. Mater.* **2004**, *14*, 693–698.

(53) Bourdo, S.; Li, Z.; Biris, A. S.; Watanabe, F.; Viswanathan, T.; Pavel, I. Structural, Electrical, and Thermal Behavior of Graphite-Polyaniline Composites with Increased Crystallinity. *Adv. Funct. Mater.* **2008**, *18*, 432–440.

(54) He, Z. W.; Lu, Q. F.; Zhang, J. Y. Facile Preparation of Hierarchical Polyaniline-Lignin Composite with a Reactive Silver-Ion Adsorbability. *ACS Appl. Mater. Interfaces* **2012**, *4*, 369–374.

(55) Yang, L.; Jiang, X.; Ruan, W.; Zhao, B.; Xu, W.; Lombardi, J. R. Observation of Enhanced Raman Scattering for Molecules Adsorbed on TiO₂ Nanoparticles: Charge-Transfer Contribution. *J. Phys. Chem. C* **2008**, *112*, 20095–20098.

(56) Lee, J.; Seo, J.; Kim, D.; Shin, S.; Lee, S.; Mahata, C.; Lee, H. S.; Min, B. W.; Lee, T. Capillary Force-Induced Glue-Free Printing of Ag Nanoparticle Arrays for Highly Sensitive SERS Substrates. *ACS Appl. Mater. Interfaces* **2014**, *6*, 9053–9060.

(57) Dutta, S.; Sarkar, S.; Ray, C.; Roy, A.; Sahoo, R.; Pal, T. Mesoporous Gold and Palladium Nanoleaves from Liquid–Liquid Interface: Enhanced Catalytic Activity of the Palladium Analogue toward Hydrazine-Assisted Room-Temperature 4-Nitrophenol Reduction. *ACS Appl. Mater. Interfaces* **2014**, *6*, 9134–9143.

(58) Bao, Z. Y.; Lei, D. Y.; Jiang, R.; Liu, X.; Dai, J.; Wang, J.; Chan, H. L. W.; Tsang, Y. H. Bifunctional Au@Pt Core–Shell Nanostructures for in situ Monitoring of Catalytic Reactions by Surface Enhanced Raman Scattering Spectroscopy. *Nanoscale* **2014**, *6*, 9063–9070.

(59) Lantman, E. M. S.; Deckert-Gaudig, T.; Mank, A. J. G.; Deckert, V.; Weckhuysen, B. M. Catalytic Processes Monitored at the Nanoscale with Tip-Enhanced Raman Spectroscopy. *Nat. Nanotechnol.* **2012**, *7*, 583–586.